The HKU Scholars Hub   The University of Hong Kong   香港大學學術庫

Title	**Charge-ordered resonating valence bond states in doped cuprates**
Author(s)	**Huang, HX; Li, YQ; Zhang, FC**
Citation	**Physical Review B - Condensed Matter And Materials Physics, 2005, v. 71 n. 18**
Issued Date	**2005**
URL	**http://hdl.handle.net/10722/43157**
Rights	**Physical Review B (Condensed Matter and Materials Physics). Copyright © American Physical Society.**

Charge-ordered resonating valence bond states in doped cuprates

Huai-Xiang Huang,[1] You-Quan Li,[1] and Fu-Chun Zhang[1,2,3]

[1]*Zhejiang Institute of Modern Physics, Zhejiang University, Hangzhou 310027, China*
[2]*Department of Physics and Center for Theoretical and Computational Physics, Hong Kong University, Hong Kong, China*
[3]*Department of Physics, University of Cincinnati, Cincinnati, Ohio 45221, USA*

We study charge ordered *d*-wave resonating valence bond states (*d*RVB) in the doped cuprates, and estimate the energies of these states in a generalized *t-J* model by using a renormalized mean-field theory. The long-range Coulomb potential tends to modulate the charge density in favor of the charge ordered RVB state. The possible relevance to the recently observed 4×4 checkerboard patterns in tunneling conductance in high-T_c cuprates is discussed.

A number of recent scanning tunneling microscopy (STM) experiments have shown spatial modulations in tunneling conductance in high-T_c cuprates.[1–5] More recent low-temperature STM experiments have reported bias-independent modulations of period approximately $4-4.5a$ (*a* denotes lattice constant) in the tunneling conductance over a wide range of energy on underdoped Bi2212 (Ref. 6) and NaCCOC.[7] Several theories have been proposed to interpret the observed checkerboard charge ordering.[8–13] Chen *et al.*[10] have proposed that the modulations are due to Cooper pair density waves. Fu *et al.*[11] have examined the possibility of a soliton crystal in a generalized Hubbard model including a nearest-neighbor Coulomb repulsion and an antiferromagnetic spin exchange coupling. Anderson[13] has proposed an explicit wave function describing a Wigner solid of holes embedded in a sea of *d*-wave resonating valence bond (*d*-RVB) states, and pointed out that the long-range Coulomb interaction furnishes the energy gain and the stiffness of the hole wave function opposes the deformation. The detailed calculations, however, have not been carried out in Ref. 13.

In the present paper, we study the charge ordered *d*RVB in the doped cuprates. We use a Gutzwiller projected wave function with both BCS pairing and charge ordering to describe the charge ordered state in cuprates. Our approach is similar to the idea outlined by Anderson,[13] who formulated the charge ordering in a *d*RVB by a site-dependent fugacity, which was introduced by Laughlin in the context of a Gutzwiller projected state in the study of the Gossamer superconductivity.[14,15] Here we shall use the renormalized mean-field theory (RMFT) developed early[16,17] to formulate charge ordering by site-dependent renormalization factors and estimate the energies of these states in the *t-J* model. We show that the long-range Coulomb potential tends to modulate the charge density in favor of the charge ordering and that the favorable patterns depend on the doping concentration. Our calculations suggest that the observed checkerboard patterns may well be induced by the long-range Coulomb repulsion, but require a rather small dielectric constant.

We consider a generalized *t-J* model with an additional long-range electron Coulomb potential,

$$H = H_{t\text{-}J} + H_c, \tag{1}$$

$$H_{t\text{-}J} = -t \sum_{\langle i,j \rangle \sigma} (c_{i\sigma}^\dagger c_{j\sigma} + \text{H.c.}) + J \sum_{\langle i,j \rangle} \mathbf{S}_i \cdot \mathbf{S}_j,$$

$$H_c = \frac{1}{2\epsilon} \sum_{i \neq j} \frac{\hat{n}_i \hat{n}_j}{r_{ij}},$$

where $c_{i\sigma}$ is an annihilation operator of a spin σ electron at site *i*. The sums in $H_{t\text{-}J}$ run over all the nearest-neighbor pairs, $n_i = \Sigma_\sigma n_{i\sigma}$, and $n_{i\sigma} = c_{i\sigma}^\dagger c_{i\sigma}$. The sum in H_c runs over all the sites of *i* and *j*. ϵ is the dielectric constant and r_{ij} is the spatial distance between the two sites *i* and *j*. A positive charge background to balance the charge neutrality is implied. There is a local constraint on every site, $\Sigma_\sigma c_{i\sigma}^\dagger c_{i\sigma} \leq 1$. In this Hamiltonian, H_c favors a charge ordering, while the kinetic energy prefers a uniform charge distribution.

We consider a variational Gutzwiller projected ground state for Hamiltonian (1),

$$|\Psi\rangle = P_G |\Psi_0\rangle, \tag{2}$$

where $P_G = \Pi_i (1 - n_{i\uparrow} n_{i\downarrow})$ is the Gutzwiller projection operator, and $|\Psi_0\rangle = \Pi_{\vec{k}} (u_{\vec{k}} + v_{\vec{k}} d_{\vec{k}\uparrow}^\dagger d_{-\vec{k}\downarrow}^\dagger)|0\rangle$ is a charge ordered BCS state, with $d_{\vec{k}\sigma} = \Sigma \alpha_{m_1 m_2} c_{\vec{k} + m_1 \vec{q}_1 + m_2 \vec{q}_2, \sigma}$. In the above expression, $(\vec{q}_1, \vec{q}_2)$ are the two wave vectors for the charge ordering (assumed to be commensurate), and $\alpha_{m_1 m_2}$ are the coefficients satisfying $\Sigma |\alpha_{m_1 m_2}|^2 = 1$ and the sums over the integers m_1 and m_2 are to extend the reduced Brillouin zone to the full original Brillouin zone.

We use the RMFT to estimate the expectation value of H in the state $|\Psi\rangle$. The RMFT was developed for the *t-J* model to study a charge homogeneous RVB state.[16,17] Here we shall extend it to the charge inhomogeneous case. We use Gutzwiller's approximation to relate the expectation values of the kinetic or spin exchange energies in the projected state $|\Psi\rangle$ (denoted by $\langle \rangle$) to the corresponding expectation values in the unprojected state $|\Psi_0\rangle$ (denoted by $\langle \rangle_0$) by two different renormalization factors g_t and g_s,

$$\langle c_{i\sigma}^\dagger c_{j\sigma} \rangle \approx g_t^{ij} \langle c_{i\sigma}^\dagger c_{j\sigma} \rangle_0,$$

$$\langle \vec{S}_i \cdot \vec{S}_j \rangle \approx g_s^{ij} \langle \vec{S}_i \cdot \vec{S}_j \rangle_0. \tag{3}$$

The renormalization factors are determined by the ratio of the probabilities of the physical process in the projected and in the unprojected states.[16–19] Similar to the method used[16] for the homogeneous case, we find

$$g_t^{ij} = 2 \sqrt{\frac{(1-n_i)(1-n_j)}{(2-n_i)(2-n_j)}},$$

$$g_s^{ij} = \frac{4}{(2-n_i)(2-n_j)}. \tag{4}$$

They depend on the electron densities at the sites i and j. In the homogeneous case, $n_i = n$, g's are independent of the sites, we recover the results in Ref. 16, $g_t^{(0)} = 2x/(1+x)$ and $g_s^{(0)} = 4/(1+x)^2$, with $x = 1-n$ the hole density. The variational calculation of the projected state $|\Psi\rangle$ in H is then mapped onto the unprojected state $|\Psi_0\rangle$ in a renormalized Hamiltonian H_{eff}, given by

$$H_{eff} = H'_{t\text{-}J} + H_c, \tag{5}$$

$$H'_{t\text{-}J} = -t \sum_{\langle i,j \rangle \sigma} g_t^{ij} (c_{i\sigma}^\dagger c_{j\sigma} + \text{H.c.}) + J \sum_{\langle i,j \rangle} g_s^{ij} \mathbf{S}_i \cdot \mathbf{S}_j.$$

Note that the intersite Coulomb interaction is not renormalized in the theory.

Similar to the procedure in Ref. 16, we introduce two mean fields: a particle-hole amplitude field $\xi_{ij} = \Sigma_\sigma \langle c_{i\sigma}^\dagger c_{j\sigma} \rangle_0$ and a particle-particle pairing field $\Delta_{ij} = \langle c_{i\uparrow} c_{j\downarrow} - c_{i\downarrow} c_{j\uparrow} \rangle_0$. The renormalized Hamiltonian can then be solved by a self-consistent mean-field theory. The energy of H_{eff} in the unprojected state, hence the energy of the generalized t-J model in the projected state, can be written in terms of the self-consistent mean fields,

$$E = -\sum_{\langle i,j \rangle} \left[2t g_t^{ij} \xi_{ij} + \frac{3J}{8} g_s^{ij} (\xi_{ij}^2 + \Delta_{ij}^2) \right] + \sum_{i \neq j} \frac{n_i n_j}{2\epsilon r_{ij}}. \tag{6}$$

In the uniformly charged dRVB state, $\xi_{ij} = \xi$ and $\Delta_{ij} = \pm\Delta$. The energy per site is found to be $E^{(0)} = -4t g_t^{(0)} \xi - (3J/4) g_s^{(0)} (\xi^2 + \Delta^2)$, where we have dropped the long-range Coulomb energy of a uniform electron density because it cancels to the energy due to the oppositely charged background.

In the inhomogeneous case, the self-consistent equations, or the Bogoliubov–de Gennes equations, are more complicated. In what follows, we shall make an approximation to replace the mean fields ξ_{ij} and Δ_{ij} by their average mean values obtained in the uniform dRVB state, and consider the effect of charge ordering on the kinetic and spin-exchange energies due to the renormalization factors g_t^{ij} and g_s^{ij}, and on the Coulomb potential. This is a rather drastic approximation, similar to what was proposed by Anderson,[13] but it should capture a substantial part of the effect of the charge ordering. This approximation may be considered as a mean-field theory with the relaxed self-consistency of the charge inhomogeneous distribution by neglecting the effect of the charge distribution to the local mean fields ξ_{ij} and Δ_{ij}. The
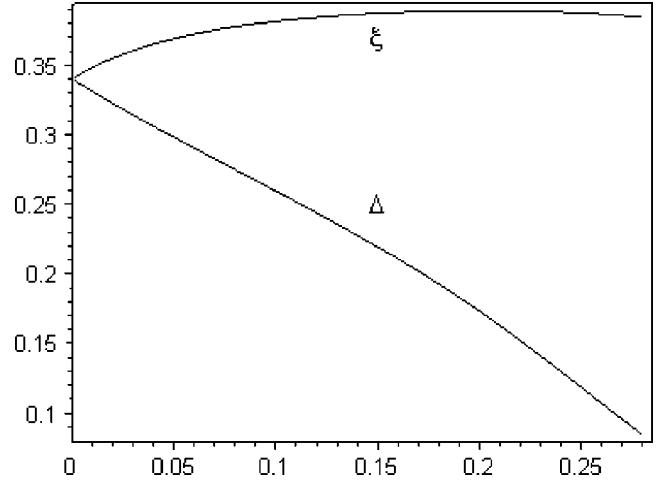

FIG. 1. The mean fields Δ and ξ vs the hole concentration x in the uniform dRVB state of the t-J model with $t/J = 3$.

variations of the local mean fields are expected to change the results quantitatively. Therefore, our results should be viewed as correct qualitatively or semiquantitatively, but not quantitatively. As we will examine later, this approximation turns out to be quite good in a limiting case where the holes are all localized. Within this approximation, the energy per site of the charge ordered dRVB state relative to the uniform dRVB state is

$$\Delta E = \Delta E_t + \Delta E_s + \Delta E_c,$$

$$\Delta E_t = (\bar{g}_t - g_t^0) \langle H_t \rangle_0 / N_s,$$

$$\Delta E_s = (\bar{g}_s - g_s^0) \langle H_s \rangle_0 / N_s,$$

$$\Delta E_c = e^2/(2\epsilon N_s) \sum_{ij} (n_i n_j - n^2)/r_{ij}. \tag{7}$$

In the above equations, $\bar{g}_{t,s} = \Sigma_{\langle ij \rangle} g_{t,s}^{ij}/2N_s$, $\langle H_{t,s} \rangle_0$ is the average kinetic (spin exchange) energy in the uniform dRVB state. In practice, we first solve the RMFT for the uniform dRVB state, from which we obtain ξ, Δ, and $\langle H_{t,s} \rangle_0$. In Fig. 1, we plot the two mean fields as functions of hole doping x for $J/t = \frac{1}{3}$. We then calculate $\bar{g}_{t,s}$ and ΔE_c for various types of charge ordering patterns to estimate the energy of the charge ordered RVB state, and to determine the optimal charge distribution. The calculation of the long-range Coulomb energy is similar to that of the Madelung constant, which converges rapidly with the appropriate choice of the summation method.

Motivated by the approximate 4×4 charge ordered states observed in STM experiments, we consider four types of parent patterns shown below with a periodicity of $4a$ along both directions in the square lattice. Each symbol represents a lattice site, and the sites marked with the same symbol have the same electron density. We restricted ourselves to the patterns with at most three different site densities. Patterns III and IV are of fourfold rotational symmetry with respect to

a diamond site. Patterns I and II are generated from the simplest two-sublattice pattern by further breaking translational symmetry by replacing some of the circle sites by diamond sites. Patterns with hole-rich sites nearby are found to have poor energy, which are not listed here. While more complicated patterns are possible, these patterns we consider here include the checkerboard and stripe ones and they should be illustrative for studying the charge ordered states.
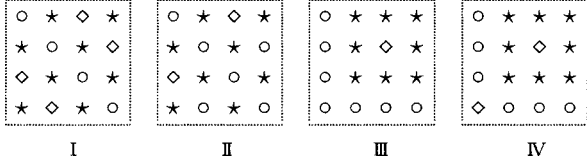
We denote $n_\diamond = n + \delta_1$, $n_\circ = n + \delta_2$, and $n_\star = n + \delta_3$. Since the overall average electron density of the system is n, only two out of the three δ's are independent. By using Eq. (4), we have $\bar{g}_{t,s}^{\mathrm{I}} = \frac{1}{2}g_{t,s}^{\diamond\star} + \frac{1}{2}g_{t,s}^{\circ\star}$, $\bar{g}_{t,s}^{\mathrm{II}} = \frac{1}{4}g_{t,s}^{\diamond\star} + \frac{3}{4}g_{t,s}^{\circ\star}$, $\bar{g}_{t,s}^{\mathrm{III}} = \frac{1}{4}g_{t,s}^{\star\star} + \frac{1}{4}g_{t,s}^{\circ\circ}$ $+ \frac{3}{8}g_{t,s}^{\star\circ} + \frac{1}{8}g_{t,s}^{\star\diamond}$, and $\bar{g}_{t,s}^{\mathrm{IV}} = \frac{1}{4}g_{t,s}^{\star\star} + \frac{1}{8}g_{t,s}^{\circ\circ} + \frac{1}{8}g_{t,s}^{\star\diamond} + \frac{1}{8}g_{t,s}^{\circ\circ} + \frac{3}{8}g_{t,s}^{\star\circ}$. Here the superscript in $\bar{g}$ indicates the type of the parent pattern, and the superscript in g refers to the two sites with the marked symbols. The Coulomb energy can be shown to be quadratic in δ's, and they are given by, in units of $e^2/\epsilon a$,

$$\Delta E_c^{\mathrm{I}} = -4.039\delta_1^2 - 4.039\delta_2^2 - 4.847\delta_1\delta_2,$$

$$\Delta E_c^{\mathrm{II}} = -1.497\delta_1^2 - 7.959\delta_2^2 - 3.468\delta_1\delta_2,$$

$$\Delta E_c^{\mathrm{III}} = -0.567\delta_1^2 - 3.772\delta_2^2 - 2.511\delta_1\delta_2,$$

$$\Delta E_c^{\mathrm{IV}} = -1.248\delta_1^2 - 4.138\delta_2^2 - 1.428\delta_1\delta_2. \tag{8}$$

Using these expressions, we have optimized the energy by varying parameters δ_1 and δ_2, and obtained charge ordered states with lower energies. These states are derivatives of the parent patterns under consideration, but may have a higher symmetry than the parent state because those sites marked with different symbols may have the same electron density. Below we shall discuss our results in three different regions of the hole concentration. In all of our calculations, we use $J/t = 1/3$, $t = 0.3$ eV, and $a = 3.8$ Å.

At the hole density around $\frac{1}{16}$, the lower-energy charge ordering pattern is $A1$ as shown in Fig. 2. There are only two types of the distinct sites in terms of the electron density in this pattern. The numerical values of the energy gain and the charge distributions are given in Table I for $x = \frac{1}{16}$ and $x = 0.05$. All other patterns at these dopings have energies either higher than or too close to the energy of the uniform dRVB state ($\Delta E > -0.01$ eV), and are not listed here. At $x = \frac{1}{16}$ and $\epsilon = 1$, the lowest-energy state has a charge distribution slightly deviated from a commensurate state with the light site completely empty ($n = 0$) and the dark site fully occupied ($n = 1$). As ϵ increases, the energy gain decreases rapidly. There is no stable charge ordering pattern at ϵ much larger than 1.5. $x = \frac{1}{16}$ is an ideal hole density for the pattern $A1$, which was also discussed in Ref. 11 and suggested in the magnetic and optical measurements.[20,21] At $x = 0.05$, the
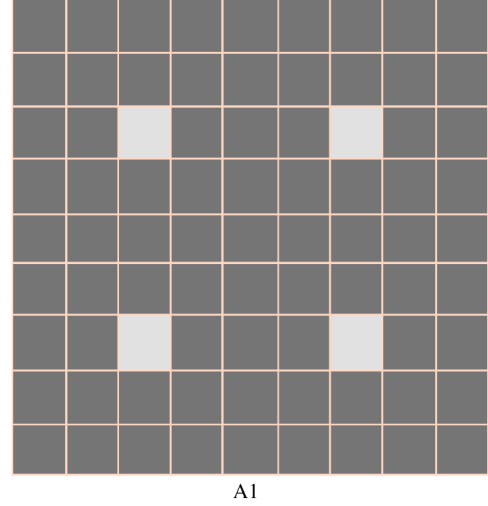

FIG. 2. Low-energy charge ordering pattern $A1$ of $4a \times 4a$ symmetry at hole density x around $\frac{1}{16}$. Shown are 9×9 patches. Each square represents a lattice site and the light (dark) square represents low (high) electron density.

pattern $A1$ is stable only for smaller ϵ, but is no longer stable for $\epsilon = 1.5$. Note that the pattern $A1$ at $x = 0.05$ is an insulator for there is no connected path for holes to move through the lattice.

At the hole density around $\frac{1}{8}$, there are several charge ordering patterns as shown in Fig. 3. Among them the favorable pattern is $B1$. Patterns $B2$ and $B4$ have three types of distinct sites in terms of the electron density, while $B1$ and $B3$ have two types of distinct sites. The energy gain and the charge distribution are given in Table II for $x = \frac{1}{8}$ and $x = 0.1$. Here we only list those patterns with relatively lower energies. As we can see from Table II, at $x = \frac{1}{8}$ the energies of patterns $B1$ and $B2$ are slightly lower than that of the homogeneous case at $\epsilon = 2$. At $x = 0.1$, the energy gain due to the charge ordering at $\epsilon = 2$ is already very tiny.

It is interesting to note that around the low hole density $x = \frac{1}{8}$, both the checkerboard pattern $B2$ and the stripe pattern[22] $B3$ are superconducting states because holes in these patterns can move through the lattice.

At high hole concentrations, several new charge ordering patterns with lower energies appear, which are shown in

TABLE I. Approximately estimated energy and charge distribution at hole density $x = 0.0625$ and $x = 0.05$. The values of an ideal hole crystal state with $n_\blacksquare = 1$ at $x = 0.0625$ are also listed for comparison.

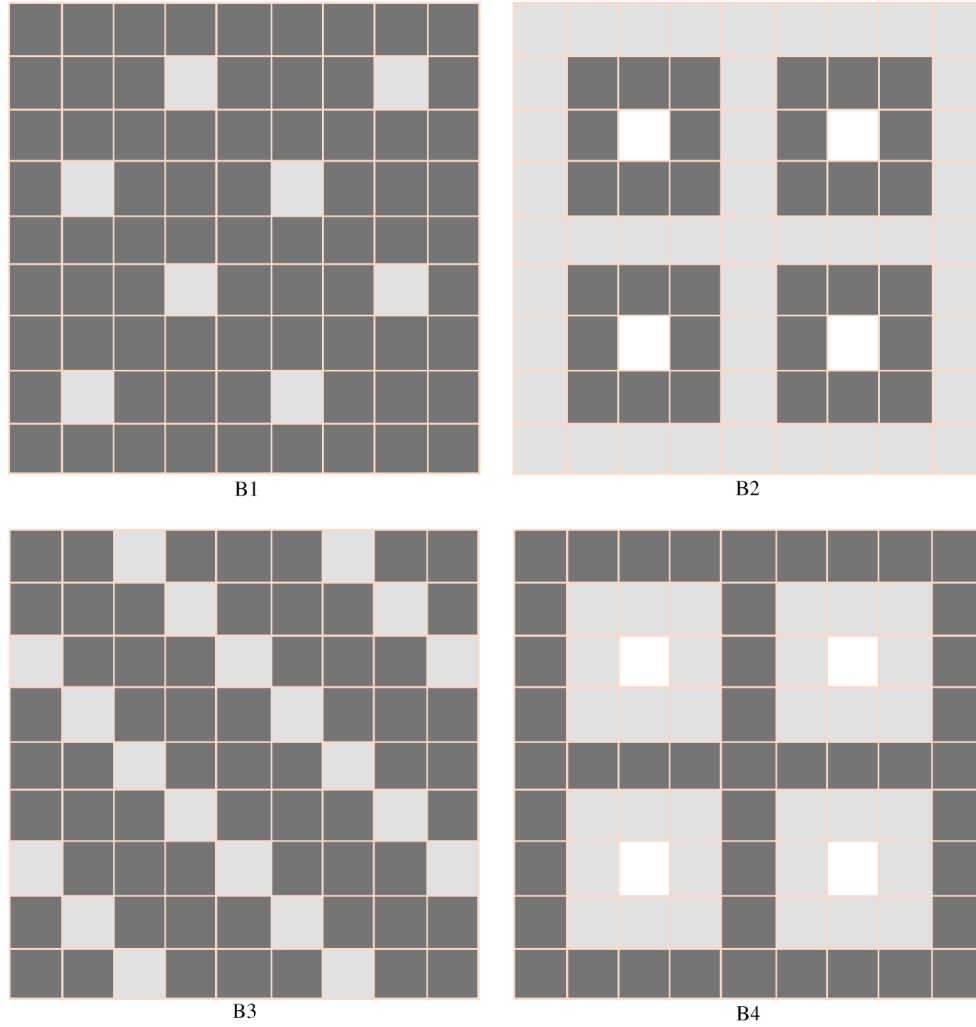| x		0.0625		0.05
ϵ	1		1.5	1
ΔE (eV)	−0.038	−0.037	−0.010	−0.016
n (gray box)	0.005	0.000	0.017	0.200
$n_\blacksquare$	0.999	1.000	0.999	1.000
Pattern	A1	A1	A1	A1

FIG. 3. Lower-energy charge ordering patterns for hole density around $x=\frac{1}{8}$. $B1$ is of a symmetry of $\sqrt{8}a \times \sqrt{8}a$, and $B3$ is a stripe.

Fig. 4. In Table III, we list the energies and charge densities of the lower-energy patterns at $x=0.15$. For $\epsilon=1$, the five patterns
($B1$, $C1$, $C2$, $C3$, and $C4$) have very close energies. In the pattern C's, the electron densities at the dark and gray sites are quite close. The empty sites in patterns $B1$ and C's form a $\sqrt{8}a \times \sqrt{8}a$ Wigner hole crystal. We do not find any lower-energy charge ordering pattern at $\epsilon > 2.5$. At $x=0.2$, the most favorable patterns are $C1$, $C4$, and the stripe pattern $B3$.

In the energy estimation for the charge ordered RVB state,

we have focused on the effect of the charge-density-dependent renormalization factors, but neglected the site dependence of the mean fields ξ and Δ. This rather crude approximation turns out to be quite good in a limiting case where all the holes are completely localized at a single site, which we analyze below. Consider pattern $A1$ at $x=\frac{1}{16}$ and pattern $B1$ at $x=\frac{1}{8}$ with the electron density n either zero or 1. In this limit, the kinetic energy vanishes. The spin exchange energy of the state can be estimated by a direct counting of the missing bonds due to the vacancies in an

TABLE II. Approximately estimated energy and charge distribution of lower-energy charge ordering patterns at hole density $x=0.125$ and $x=0.1$. Energies of some patterns with charge distribution of $n_\blacksquare=1$ are also listed for comparison.

| x	0.125										0.1				
ϵ	1			1.5		2					1			1.5	
ΔE (eV)	-0.116	-0.113	-0.056	-0.041	-0.013	-0.048	-0.043	-0.025	-0.015	-0.010	-0.059	-0.056	-0.051	-0.039	-0.021 -0.021 -0.017
$n_\square$		0.000	0.000			0.000		0.000			0.000	0.000	0.000	0.000	
n (gray box)	0.006	0.000	0.875	0.857	0.542	0.018	0.000	0.898	0.042	0.909	0.208	0.200	0.933	0.914	0.925 0.943 0.230
$n_\blacksquare$	0.999	1.000	0.984	1.000	0.986	0.999	1.000	0.964	0.994	0.954	0.999	1.000	0.984	1.000	1.000 0.975 0.996
pattern	B1	B1	B2	B2	B3	B1	B1	B2	B1	B2	B1	B1	B2	B2	B4 B2 B1

C1

C2

C3

C4
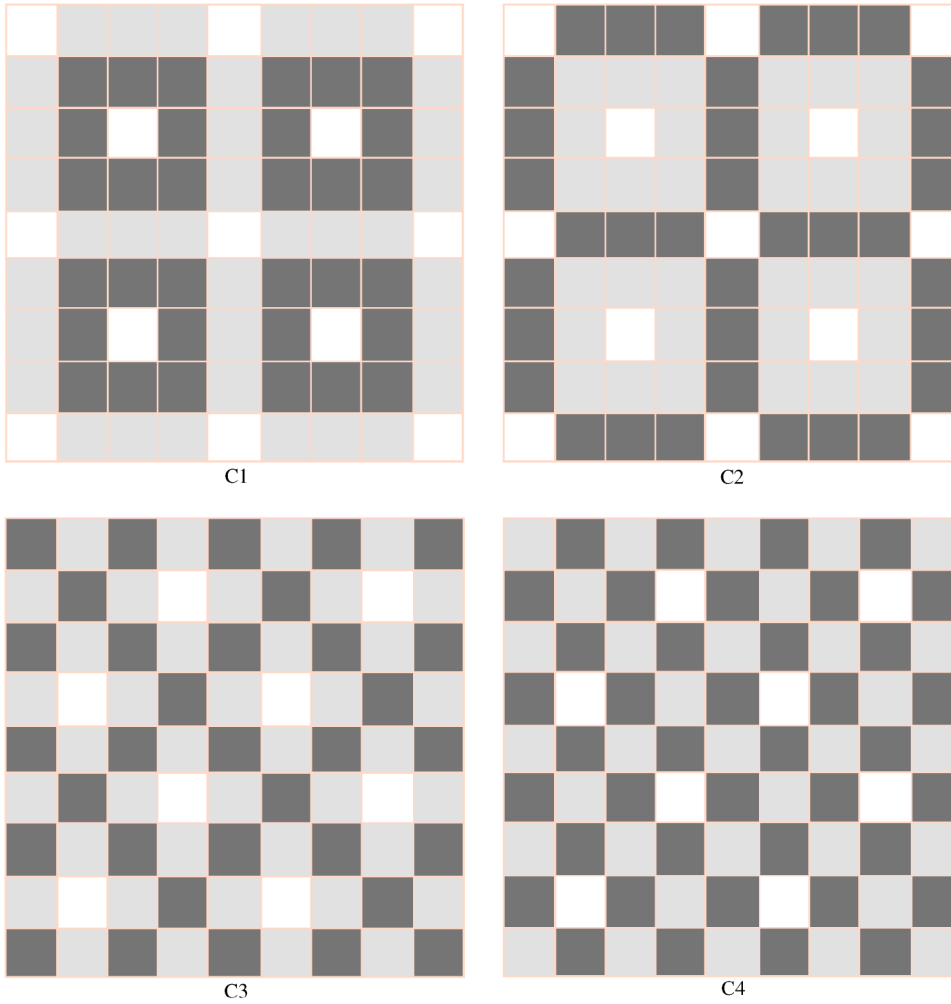
FIG. 4. Several lower-energy charge ordering patterns at $x=0.15$, not included in Fig. 3. Patterns C1 and C2 are related by the interchange of the dark and gray sites; likewise for patterns C3 and C4.

otherwise half-filled background, which is given by $E_s = 2(1-2x)\alpha$ per site, with $\alpha = -0.344J$ the spin exchange energy per bond at the half-filling. For $J=0.1$ eV, we have $E_s = -0.060$ eV at $x=\frac{1}{16}$ and $E_s = -0.052$ eV at $x=\frac{1}{8}$, which are very close to the results obtained in the present MFT: $E_s = -0.063$ eV at $x=\frac{1}{16}$ and $E_s = -0.054$ eV at $x=\frac{1}{8}$. Since the holes in the charge ordered states listed in Tables I–III are all localized or almost localized, our results based on a rather drastic approximation may not be unreasonable.

In summary, we have studied the charge ordered RVB states in the doped cuprates within a generalized t-J model by using a renormalized mean-field theory. While the kinetic energy favors a uniform charge distribution, the long-range Coulomb repulsion tends to spatially modulate the charge density in favor of charge ordered RVB states. Since both the Coulomb potential and the leading order in kinetic energy are quadratic in the density variation, we expect and indeed have found that the charge-density variation from the uniform state is always large in the charge ordered state. The stability of the charge ordered RVB state strongly depends on the dielectric constant ϵ. We do not have reliable data for the dielectric constants in Bi2212 and NaCCOC yet. Based on the optical spectra, Uchida et al.[23] have extracted $\epsilon \approx 2.5-5$ for La$_{2-x}$Sr$_x$CuO$_4$, with $\epsilon \approx 5$ at the very light doping limit $x=0.02$. Our calculation suggests that the observed charge ordered state in STM experiments in cuprates may be related to the long-range Coulomb interaction. However, the dielectric constant in cuprates might not be small enough for the

TABLE III. Approximately estimated energies and charge distributions of lower-energy charge ordering patterns at $x=0.15$.

ϵ	1								1.5				2				2.5
ΔE (eV)	−0.129	−0.113	−0.113	−0.110	−0.093	−0.062	−0.044	−0.035	−0.063	−0.048	−0.046	−0.044	−0.029	−0.148	−0.011	−0.010	−0.010
$n_\square$		0.000	0.000	0.000	0.000	0.000	0.000			0.000	0.000	0.000		0.000	0.000	0.000	
n (gray box)	0.000	0.933	0.950	0.950	0.933	0.828	0.800	0.428	0.000	0.950	0.933	0.950	0.000	0.950	0.933	0.950	0.000
$n_\blacksquare$	0.972	1.000	1.000	1.000	1.000	0.975	1.000	0.991	0.973	1.000	1.000	1.000	0.973	1.000	1.000	1.000	0.973
Pattern	B1	C1	C3	C2	C4	B2	B2	B3	B1	C3	C1	C2	B1	C3	C1	C2	B1

Coulomb interaction alone to induce the charge ordering. Among the favorable charge ordered superconducting states, pattern $B1$ has a symmetry of $\sqrt{8} \times \sqrt{8}$, patterns $B2$ and $C1$ both have checkerboard structure, and pattern $B3$ is a stripe. We do not find the bound hole pairs in the charged ordered states due to the Coulomb interaction.

[1] J. E. Hoffman *et al.*, Science **295**, 466 (2002).

[2] C. Howald, H. Eisaki, N. Kaneko, H. Greven, and A. Kapitulnik, Phys. Rev. B **67**, 014533 (2003).

[3] J. E. Hoffman *et al.*, Science **297**, 1148 (2002).

[4] K. McElroy *et al.*, Nature (London) **422**, 520 (2003).

[5] M. Vershinin *et al.*, Science **303**, 1995 (2004).

[6] K. McElroy *et al.* (unpublished).

[7] T. Hanaguri *et al.*, Nature (London) **430**, 1001 (2004).

[8] M. Franz, D. E. Sheehy, and Z. Tesanovic, Phys. Rev. Lett. **88**, 257005 (2002).

[9] Q. H. Wang and D. H. Lee, Phys. Rev. B **67**, 020511(R) (2003).

[10] H. D. Chen, O. Vafek, A. Yazdani, and S. C. Zhang, Phys. Rev. Lett. **93**, 187002 (2004).

[11] H. C. Fu, J. C. Davis, and D.-H. Lee, cond-mat/0403001 (unpublished).

[12] Z. Tesanovic, Phys. Rev. Lett. **93**, 217004 (2004).

[13] P. W. Anderson, cond-mat/0406038 (unpublished).

[14] R. Laughlin, cond-mat/0209269 (unpublished).

[15] F. C. Zhang, Phys. Rev. Lett. **90**, 207002 (2003).

[16] F. C. Zhang, C. Gros, T. M. Rice, and H. Shiba, Supercond. Sci. Technol. **1**, 36 (1988).

[17] P. W. Anderson, P. A. Lee, M. Randerai, N. Trievedi, and F. C. Zhang, J. Phys.: Condens. Matter **24**, R755 (2004).

[18] M. C. Gutzwiller, Phys. Rev. **137**, A1726 (1965).

[19] D. Vollhardt, Rev. Mod. Phys. **56**, 99 (1984).

[20] Y. H. Kim and P. H. Hor, Mod. Phys. Lett. B **15**, 497 (2001); P. H. Hor and Y. H. Kim, J. Phys.: Condens. Matter **14**, 10377 (2002).

[21] F. Zhou *et al.*, Supercond. Sci. Technol. **16**, L7 (2003).

[22] J. M. Tranquada *et al.*, Nature (London) **375**, 561 (1995); J. Zaanen and O. Gunnarsson, Phys. Rev. B **40**, R7391 (1989); V. J. Emery and S. A. Kivelson, Physica C **209**, 597 (1993).

[23] S. Uchida T. ldo, H. Takagi, T. Arima, Y. Tokura, and S. Tajima, Phys. Rev. B **43**, 7942 (1991).